American Mineralogist, Volume 81, pages 26–38, 1996

Fe ordering in kaolinite: Insights from ^{29}Si and ^{27}Al MAS NMR spectroscopy

PAUL A. SCHROEDER[1] AND ROBERT J. PRUETT[2]

[1]Department of Geology, University of Georgia, Athens, Georgia 30602-2501, U.S.A.
[2]ECC International, P.O. Box 471, Sandersville, Georgia 31082, U.S.A.

ABSTRACT

Kaolinite-rich samples were selected for ^{27}Al and ^{29}Si MAS NMR study to explore the effect of Fe on their spectra and provide insight into the nature of Fe ordering in kaolinite. Initial characterization by chemical analysis, TEM, X-ray diffraction, and magnetic mass susceptibility (χ_g) measurement was conducted to obtain five samples of high purity and with a range of Fe content. Secondary iron oxide and hydroxide phases were extracted using an HCl treatment. TEM study of the samples before and after treatment revealed the effective removal of secondary Fe phases and pristine kaolinite crystal habits.

MAS NMR experiments included measurement of ^{29}Si spin-lattice relaxation times (T_1) at 6.36 T and quantitative ^{27}Al measurements at 8.46 T. The ^{29}Si T_1 studies show a general increase in T_1 with decreasing Fe content. It is probable that the relaxation mechanism occurs dominantly through the dipole-dipole interaction with unpaired electron spins in Fe centers of the dioctahedral sheet. Data fitting indicates that spin relaxations are not best described by a single T_1. Improved fitting using double exponential or power-law behavior to describe ^{29}Si spin-relaxation phenomena indicates a heterogeneous distribution of Fe centers. The relatively longer T_1 values for two samples suggest their dioctahedral Fe domains may have a more clustered distribution within the kaolinite structure. Results from ^{27}Al studies indicate very good correlation between Fe content, χ_g, and spinning sideband (SSB) intensity. There is very little correlation between total integrated ^{27}Al intensity and Fe content. When ^{27}Al NMR intensity variations are compared with estimates of ^{27}Al NMR signal loss predicted by a paramagnetic line-broadening wipeout-sphere model that uses an idealized kaolinite structure with regularly ordered dioctahedral Fe sites, the two samples appear to have a more clustered distribution of Fe. The relative increase in SSB intensity is consistent with an increase in the number of antiferromagnetic or ferrimagnetic domains.

INTRODUCTION

Fe-bearing phases in kaolinite-rich rocks and soils have been studied from many viewpoints, particularly with regard to silicate weathering, pedogenesis, and the economic development of kaolin ores. In addition to being present in kaolinite, Fe can be found in several other phases, including oxides, hydroxides, silicates, sulfides, and organic matter. The partitioning of Fe among these various phases is often difficult to ascertain, largely because the phases often occur as intimate mixtures and in small amounts. The nature of Fe substitution within the kaolinite structure is particularly important because it is well known that the amount and ordering of isomorphous substitution can significantly affect the thermodynamic and physical properties of a mineral (Noack et al. 1993; Steefel and Cappellen 1990; Tardy and Nahon 1985). This paper will focus on the issue of Fe substitution within the kaolinite structure using new insights from nuclear magnetic resonance (NMR) spectroscopy.

There are three major impediments to the study of Fe in the kaolinite structure. The first, as mentioned above, is the intimate coexistence of kaolinite and iron oxides and hydroxides. Difficulties in separating these Fe-bearing phases from kaolinite have limited some studies in their attempt to elucidate the nature of Fe in kaolinite. This is because researchers have either (1) ignored the separation process (i.e., they assumed study material was pure kaolinite), (2) achieved only partial separation of the phases (i.e., checks were not made to ensure removal of iron oxides and hydroxides), or (3) complicated the analysis by altering the pristine state of the kaolinite structure by chemical treatments (i.e., potentially causing an oxidation-reduction reaction, dissolution of the kaolinite, or precipitation of a new phase).

The second complication in deriving true crystal-chemical structures for various kaolinite samples is the reconciliation of information from different spectroscopic and analytical techniques. To date, the analytical methods that have offered the most insight include X-ray diffraction (Brindley et al. 1986), electron spin resonance (ESR) (Mestdagh et al. 1980), Mössbauer spectroscopy (Rozenson et al. 1979), infrared spectroscopy (Mendelovici et al. 1979), electron microprobe analysis (Jepson

0003–004X/96/0102–0026$05.00

and Rowse 1975), diffuse reflectance (Malengreau et al. 1994), and selective chemical treatments (Robertson et al. 1954). Each analytical tool provides constraints needed to develop an accurate conceptual model of the crystal structure. However, there exists the problem of looking at the same object from different analytical perspectives and ensuring an unambiguous picture. The goal is to ensure that the proposed kaolinite model is consistent with the spectroscopic or analytical observations and the underlying theories and assumptions behind the technique.

The final limitation is related to the small number of Fe atoms that occupy the dioctahedral sites of natural kaolinite (≤ 3 in 100 sites). In fact, low Fe concentrations often put many spectroscopic and analytical methods at their interpretational limits (e.g., collection of a Mössbauer spectrum may take over a week).

The purpose of this paper is to provide additional insights into the nature of the ordering of Fe substitution in kaolinite using information derived from ^{29}Si and ^{27}Al NMR spectroscopy. Because the issue of coexisting Fe phases is important, this paper also addresses the effects of Fe-extraction treatments on the associated iron oxides and hydroxides in kaolinite samples as well as Fe in the kaolinite structure itself.

Samples and experimental methods

Sample selection was limited to kaolinite from relatively pure kaolin occurrences, thus ensuring easy kaolinite concentration and ample study material. Selection was also limited to samples bearing only kaolinite (i.e., halloysite-, nacrite-, and dickite-bearing kaolins were excluded). On the basis of a screening of chemical composition, particle morphology, X-ray powder diffraction (XRD), and total Fe data, five samples were selected for study. These include: (1) kaolinite in a geode from Warsaw, Illinois, U.S.A. (WR-1); (2) kaolinite from a sedimentary Cretaceous deposit in Georgia, U.S.A. (KG-1); (3) kaolinite from a sedimentary Eocene deposit in Georgia, U.S.A. (TG-1); (4) kaolinite from Pugu Hills, Dares-Salaam, Tanganyika, Tanzania, Africa (PH-1) (Yale Peabody Museum no. MIN 02.6934); and (5) a kaolinite concentrated from a tropical clay from South America (TC-1). All samples were rinsed in deionized water and size fractionated to <2.0 μm (equivalent spherical diameter) using standard centrifugation methods (Hathaway 1956).

Kaolins were prepared for chemical analysis by fusing each sample in a graphite crucible with $LiBO_2$ at 1050 °C and dissolving the resulting glass bead in a solution of 3% HNO_3 and 1% HF. Al, Ca, Fe, K, Mg, Na, Si, and Ti were assayed using a Perkin-Elmer Plasma 40 inductively coupled plasma atomic emission spectrometer (ICP-AES) calibrated using U.S. Geological Survey reference materials that bracketed the sample's elemental concentration. Loss on ignition (LOI) was determined gravimetrically by heating 1 g of sample in a muffle furnace to 1050 °C for 1 h.

The extraction of iron oxides and hydroxides without altering the kaolinite structure is critical to the analysis of Fe in kaolinite. The probable deleterious consequences of such treatments include dissolution of the silicate framework, reprecipitation of new phases, and reduction of Fe^{3+} in the kaolinite structure. For this reason, variants of a well-accepted HCl method for Fe extraction were explored. All starting materials were first examined by transmission electron microscopy (TEM) to determine the nature of the associated Fe-bearing phases and to assess the particle morphology of the kaolinite crystals. The HCl method heating times were varied from 1 to 3 h to achieve optimum results. The criteria for optimum results were determined by subsequent TEM study of the samples, looking for the presence or absence of hematite and goethite (the two Fe-bearing phases observed in this study) and the pristine crystal habit of the kaolinite (i.e., absence of solution pits and reprecipitated secondary phases).

The treatment found to be optimal for extraction of secondary Fe in this study is summarized as follows: (1) Approximately 3 g of sample was weighed (± 0.1 mg) into a 150 mL beaker; (2) 50 mL of 5.8 *N* HCl was added, heated, and maintained at 85 °C for 3 h in a water bath; (3) the sample was then immediately filtered through Whatman no. 40 filter paper into a 250 mL flask and washed with H_2O; and (4) the filtrate was then prepared and analyzed by ICP-AES to determine the dissolved Fe concentration. This method works well for kaolinite crystals. Although not discussed in this paper, the same technique was applied to halloysite, and there are TEM indications that the HCl method described above may be too aggressive for halloysite.

For comparison, extraction of Fe was also performed on the sample TG-1 using two well-accepted sodium-dithionite methods. The first method, typically used in the study of marine sediments, is detailed in Schroeder and Ingall (1994) and employs a high ratio of dithionite to sample. The second, typically used in the study of soils, is similar but uses a lower dithionite to sample ratio (1:1). In each case the soluble Fe fraction was subsequently diluted to bring concentrations into the proper range for atomic absorption analysis.

X-ray powder diffraction (XRD) was performed using a Scintag XDS-2000 diffractometer. Experimental XRD parameters included use of a Cu$K\alpha$ source, a 250 cm goniometer radius, 40 kV and 40 mA operating current, 1° and 2° primary divergence slits, 0.5° and 0.3° receiving slits, and primary and receiving Soller slits. Samples were scanned with 0.05° 2θ chopper increments at 4° 2θ/min. Both oriented and random mounts were scanned over a range from 3 to 40° 2θ. Oriented samples were prepared on quartz plates by sedimentation and drying. Diffractograms were collected in both the air-dried and ethylene glycol solvated states to ensure the presence or absence of expandable 2:1 phyllosilicate phases. Random mounts were prepared on quartz plates using an acetone slurry with precautions taken to minimize sample-displacement error.

TEM analysis was performed with a Philips 400 TEM

operated at 100 kV. Samples were prepared by sedimentation of a dilute suspension onto a 300 mesh copper grid previously prepared with a formvar coating and evaporated carbon. After drying, an evaporated carbon coat was applied.

Magnetic susceptibility measurements were made using a Johnson-Matthey balance. The balance makes a direct mass-susceptibility measurement after calibration with a known reference material [$HgCO(SCN)_4$]. The mass susceptibility is defined as the ratio of the intensity of the magnetism induced in a substance to the intensity of the applied field times the density. Units are given in cubic centimeters per gram.

^{29}Si NMR spectroscopy

All ^{29}Si spin-relaxation experiments were conducted using a 6.35 T magnet in the laboratories of Spectral Data Services, Champaign, Illinois (^{29}Si Larmor frequency = 53.762 MHz, ^{1}H Larmor frequency = 270 MHz). For all samples, initial progressive saturation experiments were conducted to get an estimate of T_1. For four of the samples that contained appreciable Fe and had inherent short T_1 values, the inversion-recovery method was employed using a standard π-$\pi/2$ pulse sequence (Fukushima and Roeder 1981). A progressive-saturation pulse sequence was used for the Fe-poor geode kaolinite WR-1. Sample rotors were spun at 4.0 kHz. Relaxation times were derived using a curve-fitting program that employs standard least-squares minimization techniques (Raner 1993). Standard proton cross-polarization (CPMAS) experiments were also conducted to determine ^{29}Si chemical shifts. The $\pi/2$ pulse times were 8.0 μs, with proton decoupling applied during acquisition and a recycle delay of 3 s.

Measurement of spin-lattice relaxation behavior is often defined as an exponential process. As properly noted by Fukushima and Roeder (1981), any scheme for the determination of relaxation times (T_1) must recognize that the actual process may not be exponential and that the T_1 values obtained may be misleading. During the inversion-recovery (IR) sequence, the π pulse inverts the spin population, whereas after τ, the $\pi/2$ recovery pulse changes from $-M_0$ to M_0. The advantage of this method is that a wide range of magnetization ($2M_0$) can be observed. If the magnetization follows a single ideal exponential decay, then relaxation after time τ can be expressed as

$$\frac{M(\tau)}{M_0} = 1 - 2\exp(-\tau/T_1). \quad (1)$$

A prerequisite of the IR method is that the magnetization fully recover after each pulse sequence (i.e., several T_1 values of waiting time are required). For the nearly Fe-free sample, WR-1, the length of time for full recovery of the magnetization was too long. Therefore, a progressive saturation sequence was employed. Under these conditions, the magnetization may follow a single ideal exponential decay. Relaxation after time τ can be expressed by the equation

$$\frac{M(\tau)}{M_0} = 1 - \exp(-\tau/T_1). \quad (2)$$

In the case of ^{29}Si [i.e., spin (I) = $\pm$½], spin-lattice relaxation largely occurs through fluctuation of the dipolar coupling of the nuclear spin with the spins of the five unpaired electrons in the 3d orbital of Fe. T_1 becomes shorter with the decrease in distance between the nucleus and the electron spin (Hayashi et al. 1992). If the nuclear spin-electron distances are too short, then the ^{29}Si nuclei signal is not usually observed because of severe line broadening and chemical shifts. When unpaired electrons are far enough away from the nuclei, spin diffusion plays a key role in the relaxation process. In this case, T_1 is related to the distance between the ^{29}Si spins and the dioctahedral sites occupied by Fe. Because ^{29}Si has an abundance of only 4.7%, and the data were collected under MAS conditions, the dipolar-coupling effect between ^{29}Si spins should be suppressed. Therefore, paramagnetic Fe substitution in kaolinite should play the dominant role in ^{29}Si relaxation. If every site within the kaolinite structure is equivalent (i.e., regular long-range ordering), then the magnetization recovers at a rate that is proportional to r_e^{-6}, where r_e is the distance between the ^{29}Si and electron spins and the number of Fe substitutions.

The assumption that the relaxation curves should obey a single exponential decay, as mentioned above, may be invalid. Blumberg (1960) showed theoretically, and both Devreux et al. (1990) and Hartman et al. (1994) showed experimentally, that the relaxation may not be a single exponential under our experimental conditions (i.e., dilute spin $\pm$½ ^{29}Si and MAS). For reasons discussed below the data were also fit using two equations. The first assumes that two time constants (one short and one long) can describe the relaxation decay. In this case a double exponential decay was used:

$$\frac{M(\tau)}{M_0} = A\exp(-\tau/T_{1s}) + B\exp(-\tau/T_{1l}) + C \quad (3)$$

where, T_{1s} and T_{1l} represent the short and long relaxation times, respectively. The second approach employs a power-law behavior. This concept was successfully used by Sen and Stebbins (1994) in the study of phase separation, clustering, and fractal characteristics in silicate glasses. In the case of a range of recovery times, recovery of the magnetization follows a power law:

$$M(t) \approx t^{\alpha} \quad (4)$$

where t is time and α is the power-law exponent. As discussed by Devreux et al. (1990) and Sen and Stebbins (1994), at short time scales the magnetization should obey the scaling relation of $M(t) \approx t^{D/6}$, where D is the fractal dimensionality of the ^{29}Si spin distribution in the material. An analysis of the fractal model has the potential to give mass-to-distance relations in real space. Application of this fractal model to relaxation phenomena and short-

range ordering problems is relatively new, and therefore fractal analysis of the data is beyond the scope of this investigation. It is, however, likely to be the subject of future studies.

^{27}Al NMR spectroscopy

The premise behind quantitation is that all ^{27}Al spins are equally detected and that the intensities are recorded in the spectral output. The ^{27}Al quantitation in silicates has been the subject of many studies (see, e.g., Alemany et al. 1991; Kirkpatrick et al. 1986; Massiot et al. 1990; Schmidt 1993; Schroeder 1993; Taulelle et al. 1992). Briefly summarized, factors that can affect intensity and resolution of spectra include those attributed to dipolar interactions, chemical-shift anisotropy, second-order quadrupolar effects (SOQE), and paramagnetic components. MAS alleviates homogeneous line broadening resulting from dipolar interactions and chemical-shift anisotropy and reduces quadrupolar effects by a factor of 3–4 (Behrens and Schnabel 1982). The magnitude of the SOQE in clays is typically small in comparison with other silicates (Ghose and Tsang 1973; Lippmaa et al. 1986; Woessner 1989), and it is likely that for the five samples examined in this study, differences in the SOQE for the octahedral site can be considered minimal. Effects on site quantitation, therefore, can be primarily attributed to the presence of Fe substituted in the octahedral site. The mechanism of homogeneous line broadening can cause substantial signal loss. The intensity of the ^{27}Al signal, therefore, depends on the distance between Fe centers and neighboring Al sites as well as on the distribution of Fe sites (i.e., concentration and ordering).

Quantitative ^{27}Al MAS NMR studies were conducted using an 8.46 T magnet (^{27}Al Larmor frequency = 94.669 MHz, ^{1}H Larmor frequency = 360 MHz). Spectra were collected at spinning speeds of 4.5 kHz, using both a CPMAS and a four-phase cycle pulse (CYCLOP) sequence. The CYCLOP spectra were used for quantitation and were collected with a pulse length of 2.2 μs (1/6 of a $\pi/2$ pulse), a recycle delay of 2 s, and 1000 acquisitions. Peak intensities were determined by an integrating routine and then normalized by the sample weight in the rotor for each experiment and the respective Al_2O_3 content.

Results

Fe removal and chemical analyses

TEM analysis revealed that the Fe-bearing minerals that are dominantly associated with kaolinite are hematite, goethite, and anatase. Figures 1a and 1b show the representative particle morphologies that are typical for the respective minerals (i.e., hexagonal hematite, acicular goethite, and tetragonal anatase), all of which have been well documented (see, e.g., Schwertmann and Taylor 1989). Also, note that the particle morphology of each kaolinite crystal before treatment is characterized by sharp pseudohexagonal faces, as shown in the high-magnification view of TG-1 (Fig. 1c). Figure 1d shows TG-1 after HCl treatment, revealing that the kaolinite structure still exhibits its sharp crystal habit.

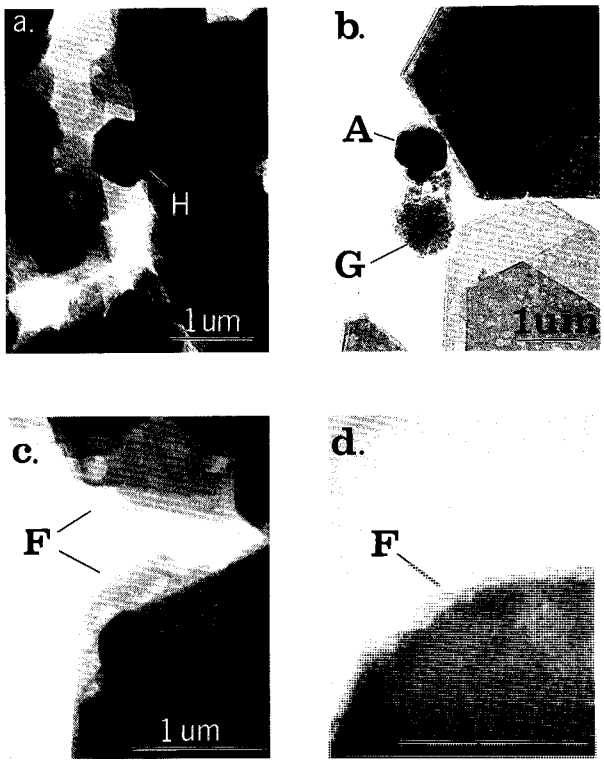

FIGURE 1. TEM photographs (a) Sample TG-1 containing hematite (H) with hexagonal habit. (b) Sample TG-1 containing goethite (G) with acicular habit, and anatase (A) with tetragonal habit. Mottling on kaolinite crystal is caused by beam damage. (c) High-magnification view of TG-1 prior to acid treatment showing sharp pseudohexagonal faces (F). (d) High-magnification view of TG-1 after acid treatment illustrating the preservation of crystal faces (F).

From TEM observations of TG-1 (not shown), it appears that both the HCl and sodium-dithionite technique of Schroeder and Ingall (1994) are effective at removing goethite and hematite. Table 1 shows the chemical analysis of each size-fractionated sample. Note that TG-1 has 0.13% extractable Fe_2O_3 with the HCl method. Results from the sodium-dithionite method of Schroeder and Ingall (1994) indicate that 0.12% Fe_2O_3 is extractable. Interestingly, when using the sodium-dithionite method with a lower extractant to sample ratio, only 0.08% Fe_2O_3 is extractable. Using TEM, hematite crystals were observed in the sample treated with the second sodium-dithionite method. These results merely substantiate the recent study of Fe-extraction methods by Raiswell et al. (1994), which showed that the HCl treatment is an efficient extraction method. The TEM results also punctuate the importance of physically looking at each sample with a high-resolution tool for the presence or absence of Fe phases after extraction treatments.

TABLE 1. Compositional, magnetic susceptibility, and X-ray diffraction data for kaolinite samples

Oxide (wt%)	TC-1	TG-1	PH-1	KG-1	WR-1
SiO_2	45.6	44.4	45.7	43.8	46.2
Al_2O_3	37.8	38.6	37.0	39.0	38.2
TiO_2	1.17	2.38	0.98	1.79	0.01
Fe_2O_3	1.81	1.11	1.31	0.38	0.11
MgO	0.01	0.03	0.03	0.02	0.24
CaO	0.01	0.03	0.02	0.07	1.10
Na_2O	0.11	0.07	0.08	0.02	0.01
K_2O	0.02	0.05	0.06	0.01	0.06
LOI	14.08	13.90	15.28	14.00	14.10
Extractable Fe (Fe_2O_3)*	0.05	0.13	0.03	0.05	0.09
		χ_g**			
Before treat.	2.20	1.20	1.40	0.02	0.45
After treat.	2.33	1.11	1.30	0.00	−0.04
χ_{Fe}†	—	78	334	40	544
		FWHM ° 2θ‡			
Before treat.	0.22	0.28	0.30	0.22	0.08
After treat.	0.22	0.26	0.30	0.23	0.08

* After HCl treatment.
** Magnetic mass susceptibility 10^{-6} emu/g in units of centimeter-gram-second.
† Calculated using Equation 5.
‡ Full-width at half-maximum for the 001 reflection measured with Cu$K\alpha$ radiation.

TEM analysis also revealed that neither of the extraction methods removes anatase. Fe^{3+} is known to substitute for Ti in the anatase structure. Therefore, any adjustments for determination of the Fe content in kaolinite must reflect this contribution. Fortunately, the TiO_2 content serves as a good quantitative measure of anatase content (Table 1). Although our unpublished high-resolution analytical TEM data for anatase from other kaolinite deposits indicate that the Fe content of anatase is variable, for the purpose of this study a constant 5% Fe for Ti substitution is assumed and employed in Fe_2O_3 corrections.

The presence of minor (<0.1%) alkali metal oxides detected in the chemical analysis suggests that extremely small amounts of smectitic or illitic clays may be admixed. No 2:1 phyllosilicates were detected with XRD; however, the detection limit for XRD is about 1%, given the experimental conditions. Additionally, the presence of alkali metals may serve for charge compensation in response to minor layer-charge imbalances present in the 1:1 layers of kaolinite itself. The slightly elevated MgO and CaO contents in WR-1 are attributed to a minor carbonate component that is removed during the acid treatment. This study assumes that contributions to the SiO_2, Al_2O_3, Fe_2O_3, and LOI measurements from nonkaolinite clay phases are negligible, and that after correction for anatase content the residual chemical analyses represent the composition of the kaolinite. The SiO_2, Al_2O_3, Fe_2O_3, and LOI measurements were normalized and are presented in Table 2, along with the structure assignments on the basis of seven O equivalents per unit formula.

TABLE 2. Normalized oxide analyses and structural formulae for kaolinite samples

Oxide (wt%)	TC-1	TG-1	PH-1	KG-1	WR-1
SiO_2	46.0	45.4	46.0	45.1	46.9
Al_2O_3	38.1	39.4	37.3	40.2	38.8
Fe_2O_3*	1.77	1.00	1.29	0.33	0.03
LOI**	14.19	14.20	15.39	14.42	14.31
		Tetrahedral			
Si	1.99	1.97	2.02	1.95	2.02
Al	0.01	0.03	0.00	0.05	0.00
Total	2.00	2.00	2.02	2.00	2.02
		Octahedral			
Al	1.96	1.98	1.93	2.01	1.97
Fe^{3+}	0.06	0.03	0.04	0.01	0.00
Total	2.00	2.01	1.97	2.02	1.97
OH	4.00	4.00	4.00	4.00	4.00
Excess H_2O†	0.05	0.05	0.25	0.08	0.06

* Fe oxide in total Fe^{2+} + Fe^{3+}.
** LOI is calculated as molar H_2O.
† Excess OH sites recast a molecular H_2O. Number of tetrahedral sites set at 2.0 and OH sites set at 4.0 assuming 7 O atoms per formula unit.

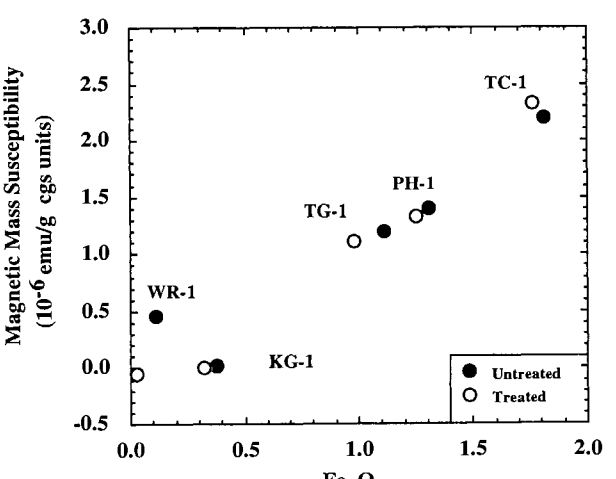

FIGURE 2. Bulk mass-magnetic susceptibility (χ_g) plotted vs. iron oxide content. Solid circles represent untreated samples. Open circles are treated samples.

TABLE 3. NMR results for kaolinite samples

	TC-1	TG-1	PH-1	KG-1	WR-1
		^{29}Si results			
Chemical shift*	−90.8	−90.9	−91.0	−91.0	−91.0
T_1 (ms)**	97	171	77	1050	20600
R^2	0.95	0.96	0.97	0.91	0.97
T_{1a} (ms)†	39	70	12	0.3	—
T_{1d} (ms)†	330	1810	158	2990	—
R^2	0.99	1.00	1.00	0.98	—
		^{27}Al results			
Chemical shift (CPMAS)‡	0.8	1.3	0.9	1.3	1.3
Chemical shift (CYCLOPS)‡	−1.2	−0.8	−1.4	−0.5	−0.4
Normalized intensity§	75	53	27	55	58
SSB/CB‖	0.27	0.17	0.21	0.09	0.07

* Relative to TMS at 0.0 ppm using CPMAS.
** Derived from fit to Equation 2, except sample WR-1, which was fit to Equation 3. R^2 = correlation coefficient.
† Derived from fit to Equation 4.
‡ Relative to 1 *M* $Al(NO_3)_3$ at 0.0 ppm.
§ Integrated using the same scaling factor and normalization by sample weight and Al_2O_3 content.
‖ Ratio of spinning side-band peak height to central-band peak height.

Mass susceptibility

Bulk mass-susceptibility (χ_g) measurements also support the removal of the hematite and goethite. Table 1 shows that for all samples, except TC-1, there is a lowering of χ_g with HCl extraction. A two-component mixing relationship is assumed to check the mass-susceptibility measurements of the extracted iron oxide (χ_{Fe}). Additional constraints to determine χ_{Fe} include a measure of the extractable iron oxide content (χ_g) and the mass susceptibility of the kaolinite (χ_k). The two-component relationship is given by

$$\chi_g = w_{Fe}\chi_{Fe} + w_k\chi_k \quad (5)$$

where, w_{Fe} and w_k are the weight fraction of iron oxide and kaolinite, respectively. The χ_{Fe} values that result from Equation 5 appear in Table 1. These values are similar to published values for iron oxides (Carmichael 1982).

The correlation between χ_k and Fe_2O_3 content after the extraction treatment (Fig. 2) supports the idea that paramagnetic properties of kaolinite are indeed imparted by the Fe in the structure. However, because the χ_g is a bulk measurement, no information about the long- or short-range ordering of the Fe in the structure can be obtained unless variable temperature experiments are conducted (Lear and Stucki 1990). The notion of Fe ordering is explored below.

^{29}Si NMR spectroscopy

The ^{29}Si chemical shifts under CPMAS conditions show a slight amount of deshielding with increasing Fe content (Table 3). Interestingly, the split in the kaolinite spectra observed by Hayashi et al. (1992) was not seen in our CPMAS spectra.

Figure 3 shows spectra for PH-1, which are representative of the ^{29}Si T_1 relaxation experiments. Figure 4a illustrates the ^{29}Si magnetization recovery (M_τ) data plotted as a function of τ for each of the five samples studied. The solid lines represent a least-squares fit for each data set using Equations 1 and 2 for the respective pulse sequences. Both a visual inspection of the plot and the correlation coefficient indicate that fitting the data with a single decay constant is not realistic. This indicates that a homogeneous relaxation mechanism is not operative in kaolinite. This observation is similar to the ^{29}Si relaxations observed by previous workers (Blumberg 1960; Devreux et al. 1990; Sen and Stebbins 1994).

As a consequence of the poor fit to a single decay scheme, a double exponential form was fitted to the data (Eq. 3). Although the theoretical basis for a fit with this form may be tenuous, the coefficients derived may serve as useful empirical parameters for correlation to other physical properties of kaolinite in future studies. This ap-

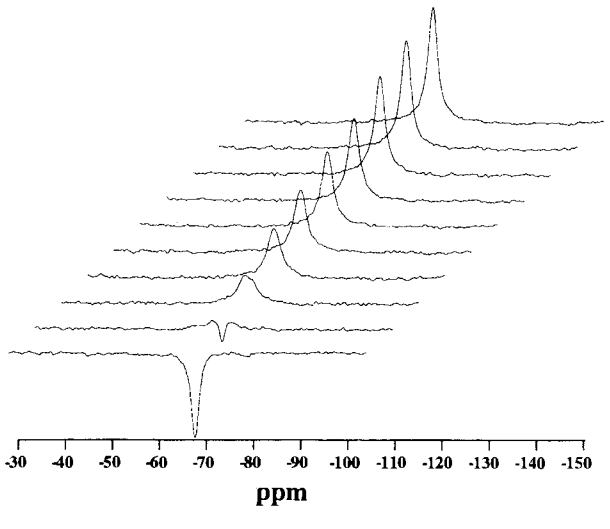

FIGURE 3. Stacked ^{29}Si MAS NMR spectra of PH-1 at 6.35 T. Data were collected using an inversion-recovery pulse sequence. Each spectrum was scanned 400 times into a free-induction decay of 4096 data points, with pulse times of π = 14 μs and $\pi/2$ = 7 μs and a recycle delay of 5 s. Waiting time (τ) for each spectrum is 10, 50, 100, 150, 200, 250, 300, 500, 750, and 1000 ms, from bottom to top.

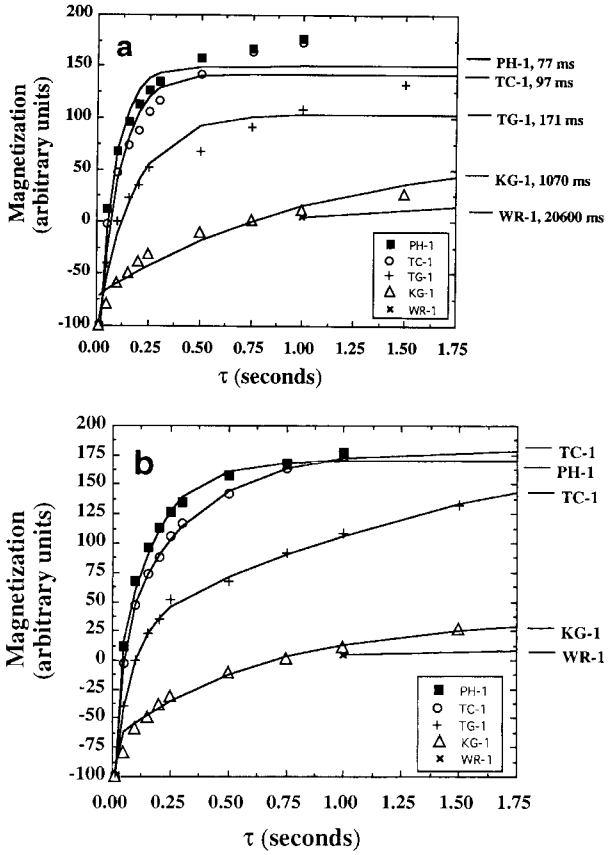

FIGURE 4. The ^{29}Si MAS NMR relaxation times (T_1). Data points are the magnetizations and waiting times (τ) measured for each kaolinite sample. (**a**) Solid lines represent the best fit using a single exponential decay function for T_1 (see Eq. 1). (**b**) Solid lines represent the best fit using a double exponential decay function for T_{1l} and T_{1s} (see Eq. 3).

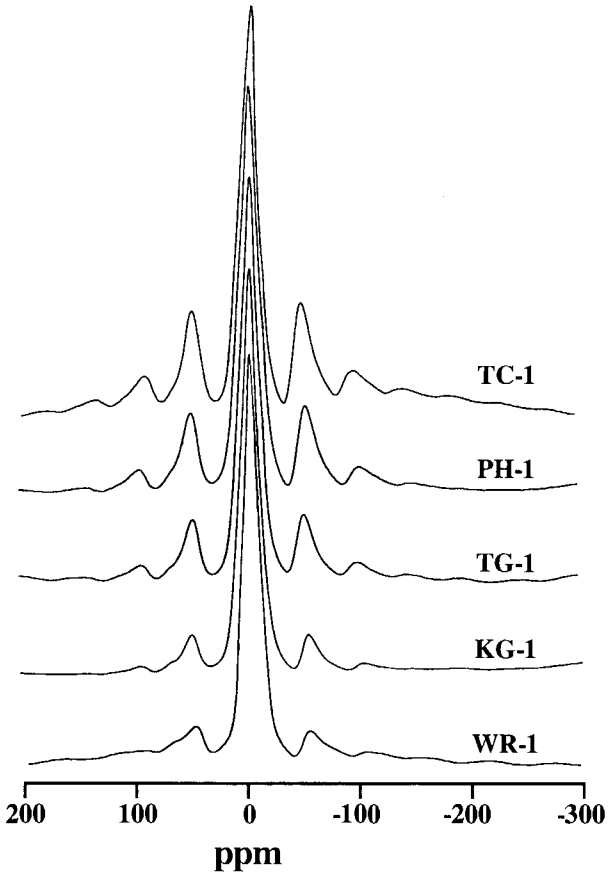

FIGURE 5. The ^{27}Al MAS NMR spectra of kaolinite samples at 8.46 T. See text for experimental conditions. Peaks found symmetrically about the main peaks are spinning side bands. Intensity scale for each spectrum was normalized to the maximum intensity observed. For relative total intensities see Table 3 and Figure 9.

proach results in two decay terms (a short T_{1s} and a long T_{1l}). The T_1 values derived from the fit are shown in Table 3, and their curves are shown in Figure 4b. As expected (partially because more independent parameters were employed), the fits and correlation coefficients are better than the single decay equations. WR-1 was not fitted with the double exponential form because its relaxation time was sufficiently long to measure with a progressive saturation experiment.

^{27}Al NMR spectroscopy

The ^{27}Al MAS NMR spectra for the five samples studied are shown in Figure 5. Table 3 shows the respective normalized ^{27}Al-integrated signal intensity (including the SSB). Except for sample TC-1, there is clearly a relationship between increasing observable signal and decreasing Fe content.

X-ray diffraction

Table 1 contains full-width at half-maximum (FWHM) diffraction data for the 001 reflection of the untreated and extracted samples. The minimal difference (<0.02° 2θ) between each treated and untreated sample is within experimental reproducibility and further suggests that the HCl extraction treatment does not significantly alter the kaolinite structure. Peak FWHM values range from 0.08 to 0.30° 2θ. The relationship between Fe content and degree of disorder mirrors that seen by Brindley et al. (1986), who found a generally positive correlation between FWHM and Fe content. Broad negative correlations are seen between ^{29}Si T_1 and FWHM as well as ^{27}Al intensities and FWHM (Tables 1 and 3).

DISCUSSION

The results of this study support the notion that Fe^{3+} substitutes for Al^{3+} in the kaolinite structure in amounts of up to 3% of the total dioctahedral sites. The results also indicate that the long-range ordering of Fe in these dioctahedral sites can be quite variable. In some cases, the long-range ordering of Fe is random, such that Fe is segregated into clustered domains, and in other cases the ordering of Fe is more regular throughout the crystal. As discussed in the Introduction, evidence for and against

the various forms of Fe associated with kaolinite comes from numerous spectroscopic, diffraction, and chemical studies. The intent of this discussion is to explore the consistencies and ambiguities between our results and interpretations derived from other studies, realizing that there may be no simple model for the kaolinite structure and that there is probably a range of structural and compositional states.

The recasting of chemical analysis into structural formulae carries the constraints of normalization into a predetermined structural model and the errors associated with correcting for associated minor phases. These corrections assume that all minor phases are accurately characterized and quantified. Alternatively, all minor phases must be removed, leaving only the kaolinite for analysis. Inaccuracies associated with characterizing the chemistry of minor phases allow for only coarse chemical corrections. Chemical removal of minor phases, on the other hand, casts uncertainty onto the pristine nature of the kaolinite crystal chemistry. In this study a combined approach was used in the hope that damage to the kaolinite structure would be minimized (through careful TEM observation) and that corrections for such phases as anatase would impart minimum error. Given these limitations, the data presented in Table 2 are reasonably accurate and hence indicate definite variations in the kaolinite compositions. The structural formulae in Table 2 unfortunately contain no information about patterns of Fe distribution within kaolinite crystals.

Jepson and Rowse (1975) were the first to suggest that kaolinite crystals may have a heterogeneous Fe content. They used an analytical TEM to examine the variance in the Fe to silica ratio among many kaolinite crystals within the same sample. They found that individual crystals showed wide variance in the Fe to silica ratio from particle to particle. Nothing can be deduced about the ordering of Fe within each crystal, but these results indicate that heterogeneity potentially exists.

^{29}Si relaxation, magnetic susceptibility, and XRD

Inspection of the ^{29}Si T_1 and T_{11} values for each sample shows a generally negative correlation in comparison with Fe content and χ_g (Fig. 6 and Tables 2 and 3). In general, the relaxation times become longer with fewer Fe atoms present. On closer inspection it is seen that TC-1 has a T_{11} two times longer than PH-1, even though more Fe is present in TC-1. A plausible explanation for this response is that the Fe in the kaolinite structure of TC-1 occurs in segregated or clustered domains. If this were the case, then there must exist domains of Si that have longer relaxations (i.e., the relaxation phenomenon is influenced by heterogeneity in the distribution of paramagnetic centers). These results are better understood in the context of the χ_g measurements.

The increase in χ_g for TC-1 after the HCl treatment is at first perplexing. If Fe^{3+} is being reduced to Fe^{2+} in the kaolinite structure, then (ignoring crystal-field effects) this would be predicted to lower χ_g because there are fewer

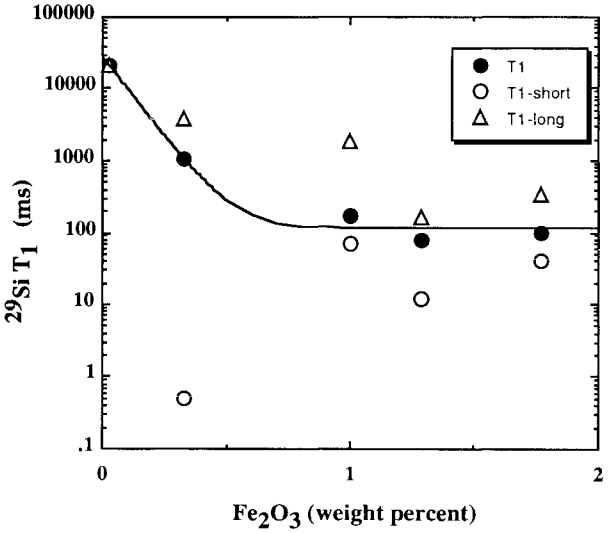

FIGURE 6. Relationship between Fe content and ^{29}Si MAS NMR relaxation times (T_1). The curve plotted on the diagram is of the form $y = a \cdot \exp(-bx) + c$ and is intended to serve only as a reference line to indicate data points that have apparent longer or shorter T_1 values.

unpaired electrons in the 3d orbitals of Fe (O'Reilly 1984). However, if crystal-field effects are considered, then several potential mechanisms may increase paramagnetism. If a ferrimagnetic component is created by the reduction of Fe^{3+} to Fe^{2+} in separate iron oxide phases, then an increase in χ_g is possible. This mechanism is similar to that which forms the magnetic domains in magnetite from the reduction of hematite in air (Carmichael 1982). Alternatively, the dehydration of γ-FeOOH can form maghemite. However, a spinel structure is necessary in each case. Each of these mechanisms also seems improbable because both transformations require temperatures much higher (1300 and 260 °C, respectively) than those experienced during the HCl extraction (85 °C). Also, discrete iron oxide phases were not observed with TEM after treatment.

An increase in χ_g may also be related to the alteration of Fe in the dioctahedral site of kaolinite. In the pretreated Fe^{3+} state, the five electrons of the Fe obey the Hund rule (i.e., they enter the orbital with identical spins) and occupy the spin-up energy levels. The crystal-field effect imparts a splitting of the electron energy levels (O'Reilly 1984). Upon reduction of some of the Fe^{3+} to Fe^{2+}, the dimension of the Fe^{2+} polyhedron probably increases because of the lower cation charge density resulting from spin pairing. If the Fe were clustered into domains, then the neighboring Fe^{3+} polyhedron should compensate by an increase in size. Under these conditions the splitting of electron energy states due to the crystal-field effect could change and potentially impart greater paramagnetic properties. It is important to note that this scenario would require isolated domains or clusters of Fe^{3+} as well as Fe^{2+} within the kaolinite structure. We feel, however, that

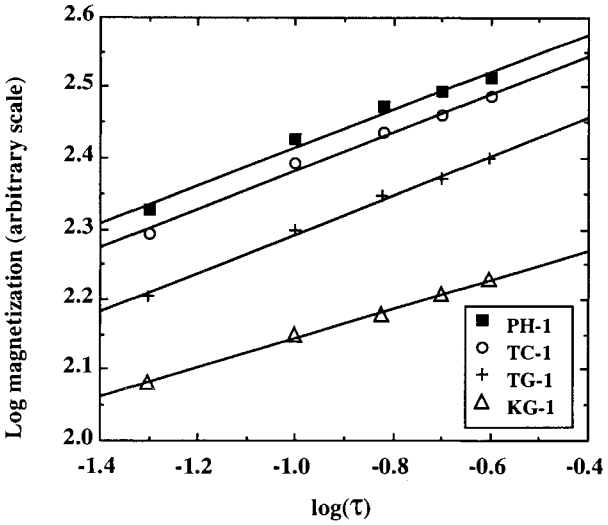

FIGURE 7. Recovery of ^{29}Si magnetization with time (τ) for kaolinite samples plotted in log-log space. Straight-line segments were fitted to the power-law regime of the recovery data shown in Figure 4.

the amount of reduced Fe in the kaolinite structure is too small to cause any of these effects.

A final possible interpretation for the change in χ_g with iron oxide removal is the magnetic-frustration hypothesis, which has been examined in smectites (Lear and Stucki 1987, 1990). If Fe occurs as clusters, the susceptibility may be due to frustrated anti-ferromagnetic behavior (i.e., electron spins of neighboring Fe atoms being in the same vectored direction; however, if spins are opposite, then the magnetization is not frustrated but behaves as a paramagnet). After treatment, removal of occluded phases may allow for improved interactions of the Fe centers with the applied magnetic field, and frustrated behavior may become less apparent. ESR spectra and variable-temperature χ_g measurements may provide insight into this matter. Unfortunately, access to such facilities was not available at the time of this study.

Previous ESR studies presented by Brindley et al. (1986) and Mestdagh et al. (1980) show good correlation between kaolin Fe content and the component of the $g = 4$ signal. The splitting observed in the $g = 4$ signal has been assigned to Fe in the dioctahedral sheet within the defect-free domains of the crystal structure (E type) and to Fe near defects near the surface of the crystals (I type). Although Brindley et al. (1986) debated the methods for apportioning the E- and I-type signals, it is clear that the relative amounts of E- and I-type signals obtained from a variety of kaolinite samples tend to group and that they do not have a single co-linear relationship (see, e.g., Fig. 2 of Mestdagh et al. 1980). In this regard the results of ESR studies are complementary to the results of this NMR study in that it is appropriate to define kaolinite by both its Fe content and the nature of Fe ordering.

The XRD data potentially allow for an assessment of the likelihood of intercalation by separate ferromagnetic domains. It is tempting to use the 001 peak widths as a direct measure of structural disorder in the c^* lattice direction. It must be remembered, however, that a powder diffraction experiment measures the diffracting effects of ca. 10^{19} discrete particles (assuming an average crystal with dimensions of $0.5 \times 0.5 \times 0.05$ μm, at 12° 2θ; see, e.g., Moore and Reynolds 1989). The FWHM is therefore a measure of a population of differently sized coherent scattering domains (CSDs), which may be unimodal or bimodal in distribution (Plançon et al. 1989). The analysis of FWHM must be approached with caution. For example, if there are two samples with the same mean CSD, one unimodal and the other bimodal, then the peak FWHM for the bimodal population (dominated by a large CSD) will be narrower than the peak for the unimodal population. This is simply because the peak height is proportional to the square of the number of CSDs (Trunz 1976).

Sample WR-1 consists of particles with extremely large CSDs (the narrowest experimental peak ever observed for a powder in our laboratory). The FWHM value of 0.08° for WR-1 is therefore principally a result of instrumental line broadening. The samples TC-1 and TG-1 exhibit FWHM values that are relatively narrow for their given Fe contents. If Fe substitution creates effectively smaller CSDs, then this suggests that TC-1 and TG-1 contain a heterogeneous CSD population. The TC-1 and TG-1 XRD data could be explained by a bimodal population of CSDs with a dominant subpopulation of crystallites containing relatively larger CSDs. If the distribution of CSDs is more homogeneous, then the FWHM would appear broader than an equivalent bimodal population with the same mean CSD. For the sample KG-1, the FWHM is wider than expected for the given Fe content. PH-1 contains the largest FWHM, suggesting that it contains the smallest mean CSD. It must be remembered, however, that the presence of Fe is not the only cause of structural defects in kaolinite. These XRD observations are at least consistent with ^{29}Si T_1 NMR and χ_g observations in that TC-1 and TG-1 can be described as having segregated domains.

Finally, evidence for the clustering of Fe domains with the dioctahedral sheets of some kaolinite samples may be obtained from the analysis of the power-law behavior of ^{29}Si relaxation recovery times. Figure 7 is a log-log plot of magnetization vs. time over the straight-line segment of the recovery curves. Only the four samples analyzed using the inversion-recovery method are shown. The slope of these lines is related to the power-law exponent α (Eq. 4). The values of α for each sample derived from a straight-line fit are 0.21, 0.27, 0.28, and 0.27 for KG-1, PH-1, TG-1, and TC-1, respectively. The period of time represented in Figure 7 is much shorter than those found by Sen and Stebbins (1994) and Devreux et al. (1990) in their studies of extremely short-range–ordered materials. The resultant fractal dimensionality is also considerably lower. A plausible explanation for these results has yet to

be made, and further relaxation studies in the light of different Fe-ordering scenarios are obviously warranted.

^{27}Al NMR and the wipeout model

The quantitative ^{27}Al data can be assessed on a relative basis using the simplified "wipeout sphere" model proposed by Schroeder (1993). This model assumes that Fe^{3+} substitutes on a regularly ordered basis for $^{[6]}$Al. The rapid decrease in signal intensity with distance of deshielding due to the presence of unpaired electrons allows for the assumption of a spherical system over which there is a radius of complete and effective paramagnetic line broadening. Using a mean-field approximation, the relative number of $^{[6]}$Al seen by the spectrometer is given by

$$I_{[6]Al} = (1 - X_{Fe})^n \quad (6)$$

where $I_{[6]Al}$ is the relative intensity of the octahedral NMR signal, X_{Fe} is the fraction of dioctahedral sites occupied by Fe^{3+}, and n is the number of neighboring sites within the wipeout sphere. Figure 8 is a two-dimensional version of the model that is intended to illustrate the wipeout concept. Medium-field magnets do not provide optimal conditions for quantitation. Therefore, the values in Table 3 are reproducible to within ±10% of the values reported. Recognizing these limitations, it is, however, still possible to bracket the effective wipeout sphere with some further assumptions about the dimensions of the kaolinite structure.

Figure 9 shows the ^{27}Al intensities of all samples normalized to TC-1 (the sample that exhibited the greatest intensity) plotted vs. X_{Fe}. Using the atomic coordinates of Young and Hewat (1988) for kaolinite (whose nonhydrogen positions are not debated), the number of dioctahedral sites at incremental 1 Å distances away from a dioctahedral center can be illustrated as in Figure 10. From this plot the total number of sites within each wipeout sphere can be ascertained. The solid lines represented in Figure 9 show the predicted ^{27}Al intensities from Equation 6 as a function of X_{Fe} for 3, 12, 25, and 100 sites within a wipeout sphere. For reference, these dines correspond to wipeout sphere radii of 4, 7, 8, and 13 Å, respectively. PH-1 exhibits the greatest ^{27}Al signal-line quenching per Fe atom, which corresponds to a wipeout sphere of about 10 Å. This is larger than the 6 Å sphere predicted by Morris et al. (1990), who studied the effect of Fe on the ^{27}Al intensity in smectites. The error associated with quantitation in our study does not allow a precise determination of the effective wipeout-sphere radius. It suffices to say, however, that the sphere's upper limit is bracketed in the range of 6–10 Å. Deviation from the model assumption of regularly ordered Fe centers would only move the relative observed ^{27}Al data points upward (i.e., fewer $^{[6]}$Al sites would be affected by the concentration of Fe). The observed data points do not follow any clear trend as predicted by the ordered model. This suggests that samples WR-1, KG-1, and PH-1 more closely approximate structures with regularly ordered Fe centers, whereas TG-1 and TC-1 better approximate structures with random long-range ordering (i.e., Fe centers can occur as clustered domains).

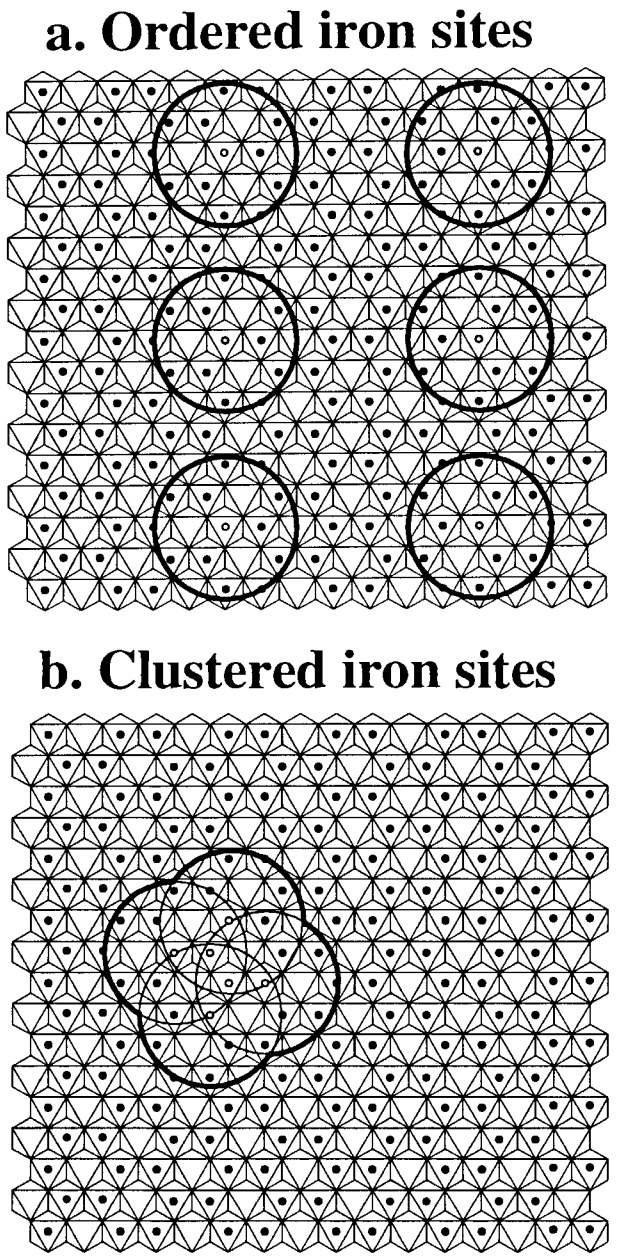

FIGURE 8. Schematic two-dimensional representations of an ideal dioctahedral sheet. Solid dots show Al sites, open dots show Fe sites. (a) Fe sites are regularly ordered in a sheet with an average Al:Fe ratio of 27:1. The bold circles represent wipeout circles with a radius of 6 Å. In this example, 56% of the Al sites are outside the circle. (b) Fe sites clustered in the sheet also have an average Al:Fe ratio of 27:1. In this scenario, 82% of the Al sites are outside the circle. The model discussed in the text is different in that it offers a three-dimensional consideration of dioctahedral sites.

It is recognized that the ordering model presented in this study represents the case of only a unimodal popu-

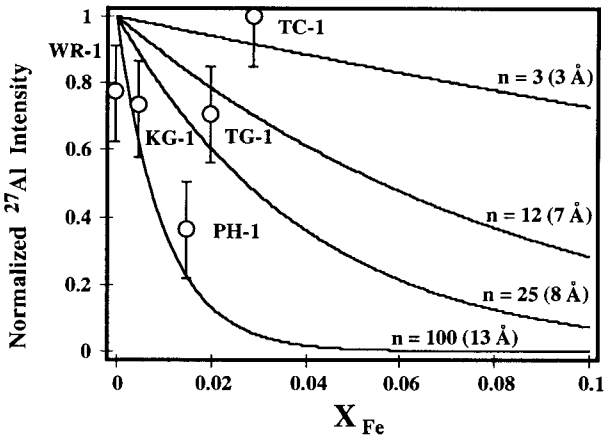

FIGURE 9. Normalized ^{27}Al MAS NMR intensity vs. the mole fraction of Fe (X_{Fe}) in the dioctahedral site. Error bars represent experimental reproducibility of measurement at 8.46 T. The lines represent the expected intensities assuming the wipeout-sphere model defined by Equation 6. The number of near neighbors in kaolinite dioctahedral sites for a given wipeout-sphere radius is equal to n (see also Fig. 10).

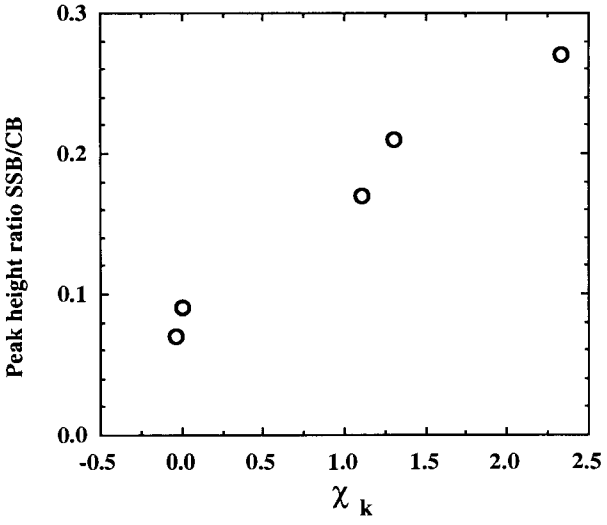

FIGURE 11. Ratio of ^{27}Al MAS NMR first-order spinning-side band (SSB) intensity to center band (CB) intensity vs. magnetic susceptibility (χ_k) for the five kaolinite samples.

lation of Fe concentration. It is likely that individual particles within the same population of a crystal have a range of Fe values (as indicated by Jepson and Rowse 1975). It is beyond the scope of this initial investigation to consider all the possible combinations of ordering schemes and Fe concentrations. This work does, however, point out the need for such a study using, for example, Monte Carlo techniques. The idea that polymodal populations of coherent scattering domains exist in kaolinite samples is certainly well founded (Plançon et al. 1989). Polymodal ordering and concentration effects clearly need to be considered.

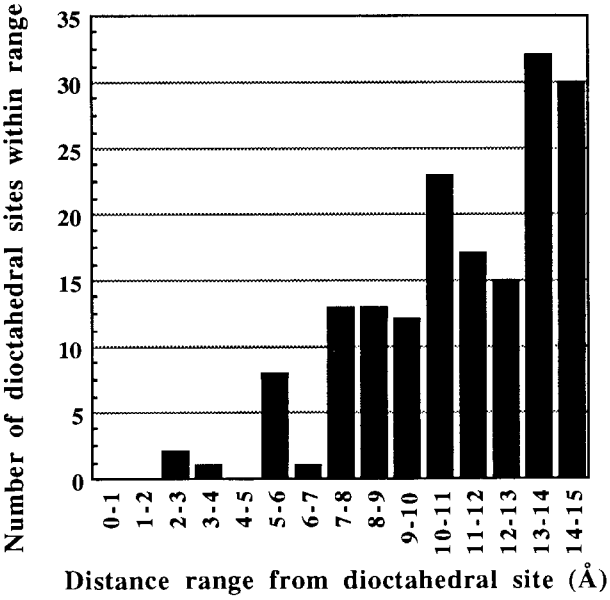

FIGURE 10. Modal frequency distribution of the number of near-neighbor dioctahedral sites that occur with 1 Å increments away from a particular dioctahedral site. See text for the assumed kaolinite lattice dimensions.

Finally, an analysis of the spinning-sideband (SSB) intensities may also give insight into the relative concentration and distribution of Fe domains. Oldfield et al. (1983) presented data that strongly indicate that the SSB observed in many natural aluminosilicates is due to large magnetic susceptibility broadening. Figure 11 shows the increase in SSB relative to the center band with increasing χ_g. This observation is consistent with the idea that discrete magnetic domains exist within each kaolinite sample. The fact that discrete domains (i.e., iron oxides and hydroxides) are not observable in our TEM study suggests that the Fe domains exist as dioctahedral Fe-rich domains that are isostructural within the kaolinite. It is still possible that ferromagnetic iron oxide domains are interlaminated within the kaolinite structure and that the TEM used in this study could not resolve their presence. Special high-resolution analytical TEM methods may be required to discern such interlaminated phases and Fe-rich dioctahedral domains. It is proposed herein that further systematic high-field quantitative ^{27}Al studies using standard additions of known ferromagnetic minerals such as goethite and hematite may provide further insight into the response of kaolinite NMR signals to discrete Fe-bearing phases.

Most studies conclude that Fe is isomorphously substituted into the dioctahedral sites. Recently, Malengreau et al. (1994), using diffuse reflectance spectroscopy, suggested that the Fe associated with kaolinite occurs as occluded ferric oxides. The basis for their conclusion is the presence of a 20000 cm^{-1} absorption band in deferrated kaolinite, a band common to discrete iron oxide and hydroxide phases. The absence of this band in synthetic Fe-

free kaolinite led them to the conclusion that Fe substitution does not occur in the kaolinite structure. Their results are consistent with our ^{27}Al SSB observations in that an increase in SSB is possible by simply physically mixing components with a large χ_g. However, the authors do not appear to entertain the possible crystal-field effect that would result when kaolinite occurs with Fe substituted into clustered domains within a dioctahedral sheet. Clearly some reconciliation between the various spectroscopic methods is needed, and future studies will be required.

Conclusions

Results of this study support the notion that long-range ordering of Fe in kaolinite can be variable and may indeed exist in segregated domains. Furthermore, direct correlation does not necessarily exist between the amount of Fe in kaolinite and the ordering of Fe within the kaolinite structure. Once criteria for recognition of variations in structural and compositional states for kaolinite are established, there may be profound implications for our understanding of geologic and pedogenic processes as well as the industrial processing of kaolin ore and its products.

Acknowledgments

Thanks are extended to ECC International for approval to publish the results and for financial support for the NMR spectroscopy. This work benefited from the insights of Jim Kirkpatrick, Nate Melear, Vernon J. Hurst, and Michael Johnson. The authors, however, are solely responsible for interpretations. Kathy Kelloes was very helpful with sample preparation for the TEM work. Kelly Kirkpatrick and Vince Brown were helpful by performing chemical analysis and sample preparation. The editorial assistance of Will Gates, Jonathan Stebbins, and two anonymous reviewers is appreciated. Partial support for this work was provided by ACS-PRF no. 29072-G2.

References cited

Alemany, L.B., Massiot, D., Sheriff, B.L., Smith, M.E., and Taulelle, F. (1991) Observation and accurate quantification of ^{27}Al MAS NMR spectra of some Al_2SiO_5 polymorphs containing sites with large quadrupole interactions. Chemical Physics Letters, 177, 301–314.

Behrens, H.J., and Schnabel, B. (1982) The second order influence of the nuclear quadrupole interaction on the central line in the NMR of quadrupolar nuclei using rapid ample spinning. Physica, 114B, 185–190.

Blumberg, W.E. (1960) Nuclear spin-lattice relaxation caused by paramagnetic impurities. Physical Review, 119(1), 79–84.

Brindley, G.W., Kao, C., Harrison, J.L., Lipsicas, M., and Raythatha, R. (1986) Relation between structural disorder and other characteristics of kaolinites and dickites. Clays and Clay Minerals, 34, 239–249.

Carmichael, R.S. (1982) Magnetic properties of minerals and rocks. In Handbook of physical properties of rocks, 2, 229–288.

Devreux, F., Boilot, J.P., Chaput, F., and Sapoval, B. (1990) NMR determination of the fractal dimension in silica aerogels. Physical Review Letters, 65(5), 614–617.

Fukushima, E., and Roeder, S.B.W. (1981) Experimental pulse NMR: A nuts and bolts approach, 539 p. Addison-Wesley, Reading, Massachusetts.

Ghose, S., and Tsang, T. (1973) Structural dependence of quadrupole coupling constant e^2qQ/h for ^{27}Al and crystal field parameter D for Fe^{3+} in aluminosilicates. American Mineralogist, 58, 748–755.

Hartman, J.S., Narayanan, A., and Wang, Y. (1994) Spin-lattice relaxation in the 6*H* polytype of silicon carbide. Journal of the American Chemical Society, 116, 4019–4027.

Hathaway, J.C. (1956) Procedure for clay mineral analysis used in the sedimentary petrology laboratory of the U.S. Geological Survey. Clay Minerals Bulletin, 3, 8–13.

Hayashi, S., Uedo, T., Hayamizu, K., and Akiba, E. (1992) NMR study of kaolinite: 2. ^{1}H, ^{27}Al, and ^{29}Si spin-lattice relaxations. Journal of Physical Chemistry, 96(26), 10928–10933.

Jepson, W.B., and Rowse, J.B. (1975) The composition of kaolinite: An electron microscope microprobe study. Clays and Clay Minerals, 23, 310–317.

Kirkpatrick, R.J., Oestrike, R., Weiss, C.A.W., Jr., Smith, K.A., and Oldfield, E. (1986) High-resolution ^{27}Al and ^{29}Si NMR spectroscopy of glasses and crystals along the join $CaMgSi_2O_6$-$CaAl_2SiO_6$. American Mineralogist, 71, 705–711.

Lear, P.R., and Stucki, J.W. (1987) Intervalence electron transfer and magnetic exchange in reduced nontronite. Clays and Clay Minerals, 35, 373–378.

——— (1990) Magnetic properties and site occupancy of iron in nontronite. Clay Minerals, 25, 3–13.

Lippmaa, E., Samoson, A., and Magi, M. (1986) High-resolution ^{27}Al NMR of aluminosilicates. Journal of the American Chemical Society, 108, 1730–1735.

Malengreau, N., Muller, J.-P., and Calas, G. (1994) Fe-speciation in kaolins: A diffuse reflectance study. Clays and Clay Minerals, 42, 137–147.

Massiot, D., Bessada, C., Courures, J.P., and Taulelle, F. (1990) A quantitative study of ^{27}Al MAS NMR in YAG. Journal of Magnetic Resonance, 90, 231–242.

Mendelovici, E., Yariv, S., and Villalba, R. (1979) Fe-bearing kaolinite in Venezuelan laterites: I. Infrared spectroscopy and chemical dissolution evidence. Clay Minerals, 14, 323–331.

Mestdagh, M.M., Vielvoye, L., and Herbillon, A.J. (1980) Fe in kaolinite: II. The relationship between kaolinite crystallinity and Fe content. Clay Minerals, 15, 1–12.

Moore, D.E., and Reynolds, R.C. (1989) X-ray diffraction and the identification and analysis of clay minerals, 332 p. Oxford University Press, New York.

Morris, H.D., Bank, S., and Ellis, P.D. (1990) ^{27}Al NMR spectroscopy of Fe-bearing montmorillonite clays. Journal of Physical Chemistry, 94, 3121–3129.

Noack, Y., Colin, F., Nahon, D., Delvigne, J., and Michaux, L. (1993) Secondary-mineral formation during natural weathering of pyroxene: Review and thermodynamic approach. American Journal of Science, 193, 111–134.

Oldfield, E., Kinsey, R.A., Smith, K.A., Nichols, J.A., and Kirkpatrick, R.J. (1983) High-resolution NMR of inorganic solids: Influence of magnetic centers on magic-angle sample-spinning lineshapes in some natural aluminosilicates. Journal of Magnetic Resonance, 51, 325–329.

O'Reilly, W. (1984) Rock and mineral magnetism, 220 p. Blackie, New York.

Plançon, A., Giese, R.F., Snyder, R., Drits, V.A., and Bookin, A.S. (1989) Stacking faults in the kaolin-group minerals: Defect structures of kaolinite. Clays and Clay Minerals, 37(3), 203–210.

Raiswell, R., Canfield, D.E., and Berner, R.A. (1994) A comparison of Fe extraction methods for the determination of degree of pyritisation and recognition of Fe-limited pyrite formation. Chemical Geology, 111, 101–110.

Raner, K. (1993) MacCurveFit v. 1.0—A program to fit use defined functions to a set of data points. Public domain software.

Robertson, R.H.S., Brindley, G.W., and Mackenzie, R.C. (1954) Mineralogy of kaolin clays from Pugu, Tanganyika. American Mineralogist, 39, 118–138.

Rozenson, I., Bauminger, E.R., and Heller-Kallai, L. (1979) Mössbauer spectra of iron in 1:1 phyllosilicates. American Mineralogist, 64, 893–901.

Schmidt, M.W. (1993) Phase relations and compositions of ion tonalite as a function of pressure: An experimental study at 650 °C. American Journal of Science, 293, 1011–1060.

Schroeder, P.A. (1993) A chemical, XRD and ^{27}Al NMR investigation of Miocene Gulf Coast shales with application to understanding illite/smectite crystal-chemistry. Clays and Clay Minerals, 41(6), 668–679.

Schroeder, P.A., and Ingall, E.D. (1994) A method for the determination

of nitrogen in clays, with application to the burial diagenesis of shales. Journal Sedimentary Research, A64, 694–697.
Schwertmann, U., and Taylor, R.M. (1989) Fe-oxides. In Minerals in soil environments, 1, 379–438.
Sen, S., and Stebbins, J.F. (1994) Phase separation, clustering and fractal characteristics in glass: A magic-angle-spinning NMR spin-lattice relaxation study. Physical Review B, 50(2), 822–830.
Steefel, C.I., and Cappellen, P.V. (1990) A new approach to modeling water-rock interaction: The role of precursors, nucleation and Ostwald ripening. Geochimica et Cosmochimica Acta, 54, 2657–2677.
Tardy, Y., and Nahon, D. (1985) Geochemistry of laterites, stability of Al-goethite, Al-hematite and Fe^{3+} kaolinite in bauxites and ferrisilcretes: An approach to the mechanism of concretion formation. American Journal of Science, 285, 865–903.
Taulelle, F., Bessada, C., and Massiot, D. (1992) Quantitative analysis of MAS NMR quadrupole nuclei. Journal de Chimie Physique, 89, 379–385.
Trunz, V. (1976) The influence of crystallite size on the apparent basal spacing of kaolinite. Clays and Clay Minerals, 24, 84–87.
Woessner, D.E. (1989) Characterization of clay minerals by ^{27}Al nuclear magnetic resonance spectroscopy. American Mineralogist, 74, 203–215.
Young, R.A., and Hewat, A.W. (1988) Verification of the triclinic crystal structure of kaolinite. Clays and Clay Minerals, 36, 225–232.

Manuscript received March 29, 1995
Manuscript accepted October 5, 1995